



**XX Fluid Mechanics Conference**



ISBN 978-83-927340-8-6

**GLIWICE**  
**17-20 September, 2012**

organized by



Polish Academy of Sciences  
Committee of Mechanics



Silesian University of Technology  
Institute of Power Engineering  
and Turbomachinery



Silesian University of Technology  
Institute of Power Engineering & Turbomachinery  
Committee of Mechanics of PAS  
Fluid Mechanics Section



---

PRACE NAUKOWE • MONOGRAFIE • KONFERENCJE Z. 29

---

# XX Fluid Mechanics Conference

## Book of Abstracts

Gliwice, 17-20 September 2012  
POLAND

Editors:  
Tadeusz Chmielniak,  
Włodzimierz Wróblewski

---

GLIWICE 2012

The book is a collection of papers which were sent to the publisher in form of doc or pdf files.  
The publisher introduced only very basic technical changes.

© Copyright by the authors of individual abstracts, 2012

Printed in Poland

ISBN 978-83-927340-8-6

First Edition

Published by Institute of Power Engineering & Turbomachinery of Silesian University of  
Technology.

Printed by D&D Ltd.  
Moniuszki Street 6, 44-100 Gliwice, Poland  
Phone: +48 230-84-24 to 26  
E-mail: druk@dd.com.pl

# Table of Contents

**17th September, Monday**

INVITED PAPERS .....	17
BLENDING THE RANS AND LES STRATEGIES FOR HIGH RE AND RA WALL-BOUNDED FLOWS, <i>Kemal Hanjalić</i> .....	19
THIN-FILM HYDRODYNAMICS IN ATOMIC FORCE MICROSCOPY, <i>Marta Krasowska</i> .....	20
CONTRIBUTED PAPERS .....	21

## **Session S1: CFD I**

WEIGHTING FUNCTION APPROXIMATION IN TRANSIENT PIPE FLOW, <i>Kamil Urbanowicz</i> .....	23
STRUCTURE MESH GENERATOR WITH ANISOTROPIC ADAPTATION FOR BOUNDARY LAYER REGION, <i>Piotr Szaltys, Jerzy Majewski, Jacek Rokicki</i> .....	24
SKEW SYMMETRIC, CONSERVATIVE FINITE DIFFERENCE SCHEMES, <i>Julius Reiss, Jens Brouwer, Jorn Sesterhenn</i> .....	26
SIMULATION OF A FREE ROUND JET WITH DISCONTINUOUS GALERKIN METHOD, <i>Maciej Marek, Artur Tyliszczak</i> .....	28

## **Session S2: Experiment I**

THE INFLUENCE OF SUCTION INTENSITY THROUGH PERFORATED WALL ON TURBULENT BOUNDARY LAYER, <i>Jan A. Szumski, Piotr Doerffer</i> .....	30
INFLUENCE OF TYPICAL FLOW DISTURBING COMPONENTS ON THE FLOW RATE IN SELECTED AVERAGING PITOT TUBES, <i>Janusz Pospolita, Mirosław Kabaciński, Sławomir Pochwała</i> .....	31
EXPERIMENTAL RESEARCH ON VELOCITY PROFILES IN SELECTED FLOW SYSTEMS, <i>Mirosław Kabaciński</i> .....	33
EXPERIMENTAL VERIFICATION OF CRITICAL FLOW MODEL OF DENSE GASES, <i>Jan Górski, Sławomir Rabczak</i> .....	35

## **Session S3: Turbulence**

SOME NEW RESULTS ON THE INFLUENCE OF TURBULENCE SCALE ON BY-PASS TRANSITION IN A BOUNDARY LAYER, <i>Joanna Jurkowska, Zygmunt Wierciński</i> .....	37
THE DECAY POWER LAW IN TURBULENCE GENERATED BY GRIDS, <i>Joanna Jurkowska, Zygmunt Wierciński</i> .....	39
AMPLITUDE MODULATED NEAR-WALL CYCLE IN A TURBULENT BOUNDARY LAYER UNDER AN ADVERSE PRESSURE GRADIENT, <i>Artur Dróżdż, Witold Elsner</i> .....	41

#### Session S16: CFD IV

HYBRID RANS/LES OF PLANE JETS IMPINGING ON A FLAT PLATE AT SMALL NOZZLE-PLATE DISTANCES, <i>Sławomir Kubacki, Jacek Rokicki, Erik Dick, Joris Degroote, Jan Vierendeels</i> .....	157
NUMERICAL SIMULATIONS FOR GAS TURBINE NOZZLE GUIDE VANE WITH FILM COOLING AND VORTEX GENERATORS JETS, <i>Paweł Flaszynski, Piotr Doerffer</i> .....	159
NUMERICAL STUDY OF THE FLOW STRUCTURE AND HEAT TRANSFER ON A ROTATING DISK SURFACE UNDER ANNULAR JET IMPINGEMENT, <i>Kamil Kieleczewski, Ewa Tułiszka-Sznitko</i> .....	161
THE EXPERIMENTAL AND NUMERICAL INVESTIGATION OF THE COANDA EFFECT AT THE FLAT PLATE, <i>Aldona Skotnicka-Siepiak, Zygmunt Wierciński</i> .....	163

#### Session S17: Multiphase flow II

MIXED MODEL FOR HEAVY PARTICLES IN LARGE EDDY SIMULATION OF TURBULENT FLOW, <i>Maria Knorps, Jacek Pozorski</i> .....	165
NUMERICAL STUDY OF PARTICLE-LADEN TURBULENT CHANNEL FLOW, <i>Marek Jaszczur</i> .....	167
CAPTURING OF INTERFACE EVOLUTION USING DIFFUSE INTERFACE METHOD, <i>Andrzej F. Nowakowski, Ahmed Balil, Shaban A. Jolgam, Franck, C.G.A. Nicolleau</i> .....	169
MEASUREMENTS OF WATER VELOCITY INSIDE THE MODEL OF THE FLOTATION MACHINE, <i>Zbigniew Buliński, Adam Mańka, Ireneusz Szczygiel</i> .....	171

#### Session S18: Flow simulation I

COLLAPSE OF N VORTICES, <i>Marek Lewkowicz, Henryk Kudela</i> .....	173
INFLUENCE OF THE ANGLE OF ATTACK ON PROPULSIVE EFFICIENCY OF OSCILLATING FOILS, <i>Tomasz Kozłowski, Henryk Kudela</i> .....	175
DECREASING STATISTICAL NOISE IN THERMAL CREEP FLOWS, <i>Newsan Sengil</i> .....	177

#### Session S19: CFD V

FAST LATTICE BOLTZMANN ALGORITHM FOR HYBRID ARCHITECTURE, <i>Lukasz Łaniewski-Wollk, Wojciech Regulski</i> .....	179
A PARALLEL MODULAR FRAMEWORK FOR MULTI-SCALE AND MULTI-PHYSICS FINITE ELEMENT SIMULATIONS OF FLUID FLOW, <i>Kazimierz Michalik, Krzysztof Banaś, Przemysław Płaszewski, Paweł Cybulka</i> .....	181
SIMPLIFIED ADAPTIVITY INDICATOR FOR EDGE BASED MESH REFINEMENT, <i>S. Gepner, J. Majewski, J. Rokicki</i> .....	183
IMPROVED EFFICIENCY OF PRESSURE-VELOCITY COUPLING ALGORITHM WITH WEAK-COMPRESSIBILITY TERMS, <i>Tomasz Dysarz</i> .....	185

## Conference Programme

Monday, September 17, 2012		Abstract	Article
Invited Lecture: Blending the RANS and LES Strategies for High $Re$ and $Ra$ Wall-Bounded Flows, Kamal Hanjalic			
Invited Lecture: Thin-Film Hydrodynamics in Atomic Force Microscopy, Marta Krasowska			
<b>Session S1: CFD I</b>			
Weighting Function Approximation in Transient Pipe Flow, Kamil Urbanowicz			
Structure Mesh Generator with Anisotropic Adaptation for Boundary Layer Region, Piotr Szalbys, Jerzy Majewski, Jacek Rakicki			
Skew Symmetric, Conservative Finite Difference Schemes, Julius Reiss, Jens Brouwer, Iörn Sesterhenn			
Simulation of a Free Round Jet with Discontinuous Galerkin Method, Maciej Marek, Artur Tyliczka			
<b>Session S2: Experiment I</b>			

Wednesday, September 19, 2012		Abstract	Article
Invited Lecture: Multiphase Flow Simulations in the Upper Airways and Tracheobronchial Geometries of the Lung, Chris Lacor			
Invited Lecture: Methods of Spatio-Temporal Data Analysis, Vaclav Uroba			
Invited Lecture: Revisiting Near Wall Turbulence Physics, Michel Stanislas			
<b>Session S16: CFD IV</b>			
Hybrid RANS/LES of Plane Jets Impinging on a Flat Plate at Small Nozzle-Plate Distances, Slawomir Kubacki, Jacek Rakicki, Erik Dick, Joris Degroote, Jan Vierendeels			
Numerical Simulations for Gas Turbine Nozzle Guide Vane with Film Cooling and Vortex Generators Jets, Pawel Flaszynski, Piotr Doerffer			
Numerical Study of the Flow Structure and Heat Transfer on a Rotating Disk Surface Under Annular Jet Impingement, Kamil Kielcowski, Ewa Tulska-Szvitko			
The Experimental and Numerical Investigation of the Coanda Effect at the Flat Plate, Aldona Skotnicka-Siepsiak, Zygmunt Wiercinski			

## **HYBRID RANS/LES OF PLANE JETS IMPINGING ON A FLAT PLATE AT SMALL NOZZLE-PLATE DISTANCES**

Slawomir KUBACKI<sup>1</sup>, Jacek ROKICKI<sup>1</sup>, Erik DICK<sup>2</sup>, Joris DEGROOTE<sup>2</sup>,  
Jan VIERENDEELS<sup>2</sup>

<sup>1</sup>*Institute of Aeronautics and Applied Mechanics, Warsaw University of Technology,  
Nowowiejska 24, 00-665, Warsaw, Poland;* <sup>2</sup>*Department of Flow, Heat and Combustion  
Mechanics, Ghent University, St.-Pietersnieuwstraat 41, B-9000, Ghent, Belgium.*

E-mail: jack@meil.pw.edu.pl

### *Abstract*

A  $k-\omega$  based hybrid RANS/LES (Reynolds Averaged Navier Stokes/Large Eddy Simulation) model is tested for simulation of plane impinging jets at various nozzle-plate distances ( $H/B$ , where  $H$  is the distance and  $B$  is the slot width) and various Reynolds numbers (based on the slot width and the velocity in the symmetry plane). The studied combinations are  $H/B=2$  for  $Re=10000$ ,  $H/B=4$  for  $Re=18000$  and  $H/B=9.2$  for  $Re=20000$ . The focus is on small distance of the nozzle exit to the plate. This means for impact of the jet onto the plate before complete mixing of the shear layers. The centre of the impact zone is then in laminar state and the developing boundary layer on the plate undergoes transition to turbulent state. The transitional flow cannot be correctly simulated with a RANS turbulence model, but we will demonstrate that a hybrid model is basically correct. The test case with the large nozzle-to-plate distance ( $H/B=9.2$ ) is only meant to demonstrate the correct setting of the inflow conditions. The reliability of the hybrid model will be demonstrated by comparing results of mean velocity profiles, profiles of fluctuating velocity components and skin friction on the plate with results from LES using a dynamic Smagorinsky model and experiments. In LES mode, the hybrid RANS/LES model uses two definitions of the local grid size, one based on the maximum distance between the cell faces in the destruction term of the turbulent kinetic energy equation and one based on the cube root of the cell volume in the eddy-viscosity formula. This allows accounting for flow inhomogeneity on anisotropic grids. Under the assumption of local equilibrium, the eddy viscosity of the hybrid model reduces to a Smagorinsky subgrid viscosity with the usual constant  $C_s=0.1$ . In RANS mode, the hybrid model turns into the newest version of the  $k-\omega$  model by Wilcox (Formulation of the  $k-\omega$  turbulence model revisited, AIAA Journal 46, pp. 2823-2837, 2008).

*Key words:* turbulence modelling, plane impinging jet, hybrid RANS/LES model, Large Eddy Simulation

### **INTRODUCTION**

Plane impinging jets were studied experimentally (Tu and Wood, 1996, Sakakibara et al., 1997, Ashforth-Frost et al., 1997, Zhe and Modi, 2001, Guo and Wood, 2002, Narayanan et al., 2004, Dogruoz, 2005, Senter and Sollic, 2007) and numerically using LES (Cziesla et al., 2001, Beaubert and Viazzo, 2003, Tsubokura et al., 2003) in order to provide a database for assessment of the qualities of turbulence models, to study the influence of the inlet conditions on the impingement plate shear stress and heat transfer distributions and to understand the relationship between heat transfer and shear stress along the plate. DNS were performed (Tsubokura et al., 2003, Hattori and Nagano, 2004) to clarify the effect of the inlet

disturbances on the flow and heat transfer characteristics along the impingement plate or to study the effect of nozzle-plate distance on the location of the secondary peak in the shear stress and the heat transfer profiles. The predictive qualities of various RANS models were verified by (Fernandez et al., 2007) and (Jaramillo et al., 2008), among others, for plane impinging jets at various nozzle-plate distances and Reynolds numbers. For large nozzle-plate distance, RANS models suffer from difficulties in reproducing the turbulence mixing in the developing shear layers of the jet as well as in capturing the correct level of shear stress and heat transfer in the impact zone. This poses a difficulty in application of the RANS-based techniques in analysis of complex flow systems in which free jet development and its subsequent impingement largely determine the level of the wall shear stress and local heat transfer rate along the impingement wall. For small nozzle-plate distance, where the flow in the impact zone physically is laminar, the prediction of the shear stress and heat transfer levels in the impact zone are basically correct with RANS models due to use of stress limiters which damp most of the turbulence in the impact zone. The transition from laminar to turbulent state in the developing boundary layer on the plate is completely ignored by RANS models.

In the present work, a  $k-\omega$  based hybrid RANS/LES model and the  $k-\omega$  RANS model of (Wilcox, 2008) are employed to study their applicability in reproducing the plane impinging jet flow characteristics at low nozzle-plate distances ( $H/B=2$  and  $4$ ) and at various Reynolds numbers ( $10000$  and  $18000$ ). The correctness of specifying the inlet conditions is verified for the case  $H/B=9.2$ ,  $Re=20000$ . The numerical results obtained with the hybrid and RANS models are compared with experimental data and LES using the dynamic Smagorinsky model.

The hybrid RANS/LES model analysed here belongs to the class of unified DES-type approaches, as first proposed by (Strelets, 2001). For a classification of hybrid approaches, we refer to (Fröhlich and von Terzi, 2008). The local grid size, replacing the turbulent length scale in the LES mode of the hybrid model, is introduced in both the destruction term of the turbulent kinetic energy equation and in the eddy-viscosity formula, according to methods first proposed by (Davidson and Peng, 2003, Kok et al., 2004, and Yan et al., 2005), In RANS mode, the newest version of the  $k-\omega$  model of Wilcox (2008) is recovered. Two definitions of the local grid size are used to better account for flow inhomogeneity on anisotropic grids. The model was already tested on round impinging jets (Kubacki and Dick, 2011). A simpler version was tested on plane impinging jets at large nozzle-plate distances by (Kubacki and Dick, 2010).

## THE HYBRID RANS/LES MODEL

The transport equations for the turbulent kinetic energy,  $k$ , and the inverse of the turbulent time scale (frequency),  $\omega$ , read:

$$\frac{\partial k}{\partial t} + \frac{\partial(U_j k)}{\partial x_j} = \tau_{ij} \frac{\partial U_i}{\partial x_j} - \max\left(\beta^* k \omega, \frac{k^{3/2}}{C_{DES} \Delta}\right) + \frac{\partial}{\partial x_j} \left[ \left( \nu + \sigma^* \frac{k}{\omega} \right) \frac{\partial k}{\partial x_j} \right], \quad (1)$$

$$\frac{\partial \omega}{\partial t} + \frac{\partial(U_j \omega)}{\partial x_j} = \alpha \frac{\omega}{k} \tau_{ij} \frac{\partial U_i}{\partial x_j} - \beta \omega^2 + \frac{\sigma_d}{\omega} \frac{\partial k}{\partial x_j} \frac{\partial \omega}{\partial x_j} + \frac{\partial}{\partial x_j} \left[ \left( \nu + \sigma \frac{k}{\omega} \right) \frac{\partial \omega}{\partial x_j} \right]. \quad (2)$$

In these equations,  $\nu$  is the kinematic molecular viscosity, and the modelled stress tensor and the shear rate tensor are  $\tau_{ij}=2\nu_t S_{ij}-2/3k\delta_{ij}$  and  $S_{ij}=1/2(\partial U_i/\partial x_j+\partial U_j/\partial x_i)-1/3(\partial U_k/\partial x_k)\delta_{ij}$ , respectively. The local grid size  $\Delta$  is defined by  $\Delta=\max(\Delta_x, \Delta_y, \Delta_z)$  where  $\Delta_x, \Delta_y, \Delta_z$  denote the distances between the cell faces in  $x, y$  and  $z$  directions. The grid size is multiplied with a tuning constant  $C_{DES}$ , which we derive later. The basic model is the  $k-\omega$  RANS of (Wilcox, 2008). The motivation for the modification of the destruction term in (1) is that the dissipation



in the k- $\omega$  RANS model is  $\varepsilon=\beta^*k\omega=k^{3/2}/L_t$ , where the turbulent length scale is  $L_t=k^{1/2}/(\beta^*\omega)$ . So, it means that in the dissipation term, the turbulent length scale is replaced by the grid size when the model transfers to LES mode. The choice of the grid size measure is crucial in any LES like formulation (Scotti et al, 1993, Spalart et al, 2006, Fröhlich and von Terzi, 2008). The literature shows that there is a preference for the maximum size in a DES formulation (Yan et al, 2005, Spalart et al, 2006), while there is a preference for the cube root measure in an LES formulation (Scotti et al, 1993, Fröhlich and von Terzi, 2008). For the length scale in the k-equation (1), we take the maximum size, as by the substitution of the length scale, a DES model is obtained, in the style as first proposed by (Strelets, 2001).

The closure coefficients are (Wilcox, 2008):

$$\begin{aligned} \beta^* &= 0.09, \quad \alpha = 0.52, \quad \beta = \beta_0 f_\beta, \quad \beta_0 = 0.0708, \\ \sigma &= 0.5, \quad \sigma^* = 0.6, \quad \sigma_{do} = 0.125, \\ f_\beta &= \frac{1+85\chi_\omega}{1+100\chi_\omega}, \quad \chi_\omega = \frac{|\Omega_{ij}\Omega_{jk}S_{ki}|}{(\beta^*\omega)^3}, \quad \sigma_d = \begin{cases} 0 & \text{for } \frac{\partial k}{\partial x_j} \frac{\partial \omega}{\partial x_j} \leq 0 \\ \sigma_{do} & \text{for } \frac{\partial k}{\partial x_j} \frac{\partial \omega}{\partial x_j} > 0 \end{cases} \end{aligned}$$

where  $\Omega_{ij}=1/2(\partial U_i/\partial x_j-\partial U_j/\partial x_i)$  is the vorticity tensor.

The eddy-viscosity is defined according to (Davidson and Peng, 2003 and Kok et al., 2004) by

$$\nu_t = \min\left(\frac{k}{\omega}, \beta^* C_{DES} \sqrt{k} \Delta_{LES}\right), \quad (3)$$

where  $\Delta_{LES}=(\Delta_x\Delta_y\Delta_z)^{1/3}$ . The motivation for this modification is that the RANS eddy viscosity is  $\nu_t=\beta^*L_tk^{1/2}$ . So, it means that also in the eddy viscosity expression, the turbulent length scale is replaced by the grid size. The chosen grid size is here the cube root measure, so the typical LES grid size. The grid size is multiplied with the tuning constant  $C_{DES}$ . The justification for using different grid scales in Eq. (3) and in the k-equation (Eq. 1) is that, under local equilibrium (production of k equal to dissipation of k), the eddy viscosity reduces in LES mode to a Smagorinsky subgrid viscosity

$$\nu_t = \left( C_s \Delta_{LES} \left( \frac{\Delta}{\Delta_{LES}} \right)^{1/4} \right)^2 S. \quad (4)$$

with  $C_s=(\beta^*)^{3/4}C_{DES}$  set to the usual value 0.1, which gives  $C_{DES}=0.6086$  and with the magnitude of the shear rate  $S=(2S_{ij}S_{ij})^{1/2}$ . The role of the term  $(\Delta/\Delta_{LES})^{1/4}$  is to increase the eddy viscosity on high aspect ratio cells, with respect to the value obtained by the cube root grid size in all turbulence length scale substitutions. We follow here the approach by (Scotti et al., 1993), who proved much better predictive qualities of LES on anisotropic grids by an increased eddy viscosity.

For the RANS simulations (Wilcox, 2008), a stress limiter is applied. This means that the turbulent viscosity  $\nu_t$  is defined by

$$\nu_t = \frac{k}{\omega}, \quad \tilde{\omega} = \max\left(\omega, C_{lim} \sqrt{\frac{2S_{ij}S_{ij}}{\beta^*}}\right) \quad (5)$$

with  $C_{lim}=7/8$ . The RANS stress limiter (Wilcox, 2008) is omitted in Eq. (3) in the hybrid RANS/LES model. Tests showed that the stress limiter has only negligible effect on the results of impinging jet flows with the hybrid RANS/LES model. The limiter is only significant for the RANS model.

As boundary conditions,  $k=0$  at walls and  $\omega=u_\tau^2 S_R/\nu$  in the centre of a cell at a wall, with  $u_\tau=(\tau_w/\rho)^{1/2}$ ,  $\tau_w=\mu \cdot S$ ,  $S_R = \min[(200/k_s^+)^2, 6/(\beta_0(\Delta y^+)^2)]$ , where  $\Delta y^+=\Delta y \cdot u_\tau/\nu$ ,  $k_s^+$  is a

dimensionless roughness height,  $\Delta y$  is the distance to the wall of the centre of the cell,  $\rho$  is the fluid density and  $\mu$  is the dynamic molecular viscosity. Since the wall is assumed to be hydraulically smooth, the dimensionless roughness height was set to  $k_s^+ = 4$ , according to (Wilcox, 2008).

## COMPUTATIONAL FRAMEWORK

The computational domain consists of a rectangular box as shown in Fig 1. Details related to the size of the computational domain, coordinate system, boundary conditions and the number of grid points are given in Table 1.

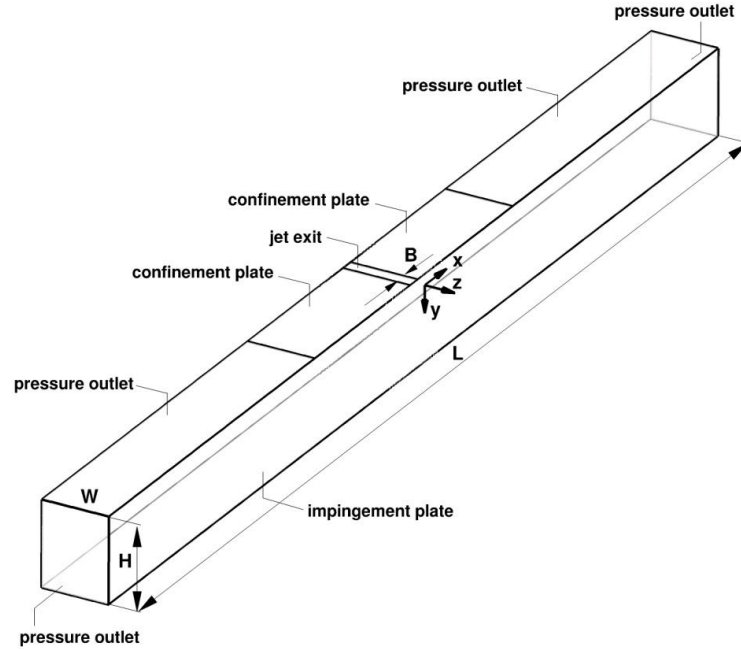


Figure 1. Sketch of computational domain, coordinate system and boundary conditions for plane impinging jet simulation at  $H/B=4$ . Periodic conditions are imposed in the  $z$  direction.

At the inlet to the computational domain (jet exit) an almost flat mean velocity profile was specified by

$$V(x,0,z) = V_0(1 - (2x/B)^{14}), \quad (6)$$

where  $V_0$  denotes the mean velocity in the symmetry plane. We show later that the mean velocity profile given by Eq. (6) corresponds well with experimental data immediately downstream of the slot. For all cases in Table 1, the turbulence intensity at the jet exit was set to  $Tu=0.9\%$  in accordance with the experiments of (Zhe and Modi, 2001). A similar value of the inlet turbulence intensity, 1%, was used by (Ashforth-Frost et al., 1997). We use also the measurements by (Ashforth-Frost et al., 1997) for comparison with our numerical results (the experimental set-up by Ashforth-Frost et al, 1997, is very similar to the experimental set-up by Zhe and Modi, 2001).

The integral length scale was not measured in the inlet plane by (Zhe and Modi, 2001) and (Ashforth-Frost et al., 1997). In the present RANS computations, constant values of  $k$  and  $\omega$  were specified at the inlet of the computational domain with  $Tu=0.9\%$ , while the turbulent (integral) length scale  $l_t$  was specified according to (Jaramillo et al, 2008), namely  $l_t=0.1667B$ . Uniform inlet profiles of the turbulent quantities are specified by  $k=1.5(Tu \cdot V_0)^2$  and  $\omega=k^{1/2}/(\beta^* l_t)$ . For the hybrid simulations, the vortex method of Fluent was used to generate the resolved fluctuations in the inlet plane (Mathey et al, 2006). For the LES, random fluctuations were generated in the inlet plane. The full RANS profiles of  $k$  and  $\omega$  were imposed at the jet

exit to reproduce the resolved perturbations. With the vortex method, structures smaller than the grid size are not generated. So, the modelled part of the total fluctuating velocity is automatically not taken into account. The modelled  $k_{SGS}$  and  $\omega_{SGS}$  are prescribed by  $k_{SGS}=(C_{DES}\Delta)^{2/3}\varepsilon^{2/3}=(\beta^*k\omega C_{DES}\Delta)^{2/3}$ ,  $\omega_{SGS}=\varepsilon/(\beta^*k_{SGS})=\omega k/k_{SGS}$  (Kubacki and Dick, 2011). This means that the length  $C_{DES}\Delta$  is used as representative length scale for the subgrid turbulence. The top boundary, at the height of the jet exit, was split into two parts. A confinement wall was specified for a part of the boundary extending from the slot edges up to the streamwise distance  $x/B= \pm 13$  (Zhe and Modi, 2001). A pressure outlet boundary condition was applied for the remaining part of the top boundary as well as in the outflow planes located at  $x/B= \pm 40$ . This means that static pressure was prescribed (set here to zero), as well as the direction of the backflow (which is determined here in the cells adjacent to the boundary) and the values of the transported scalars. With the pressure outlet condition imposed, a very low value of the turbulent/subgrid to molecular viscosity ratio was prescribed in the flow regions re-entering the computational domain (set here to 0.01) while the backflow turbulent length scale was set to  $l_t=0.1667B$ . No fluctuations were generated with the vortex method at the pressure outlet boundaries with the LES and hybrid RANS/LES models. Periodic boundary conditions have been applied in the spanwise  $z$ -direction.

Table 1

Length  $L$ , height  $H$  and width  $W$  of the computational domains for simulations performed with the hybrid RANS/LES and LES models and the number of cells  $N_x, N_y, N_z$  in  $x, y$  and  $z$  directions.

Case	L/B	H/B	W/B	$N_x$	$N_y$	$N_z$	$N_{tot}$ (M)
H/B=9.2, Re=20000	80	9.2	$\pi$	320	320	70	7.2
H/B=4, Re=18000	80	4	$\pi$	320	180	70	4.0
H/B=2, Re=10000 (basic)	80	2	$\pi$	320	110	70	2.5
H/B=2, Re=10000 (fine)	80	2	$\pi$	540	200	140	15.1

The computations using the RANS and the hybrid RANS/LES models have been performed with the Fluent code ver. 13, while the LES simulations have been performed with OpenFOAM. In Fluent, the transport equations (Eqs. 1-2) were implemented with the user-defined scalar functionality. For the hybrid RANS/LES, a TVD-bounded central scheme was applied to the convective terms in the momentum equations, while for LES it was the central differencing scheme with filtering of high-frequency ripples. The second order upwind scheme was used to the convective terms in the  $k$ - and  $\omega$ -equations (hybrid RANS/LES). For RANS, the second order upwind scheme was used for discretisation of the convective terms in all equations. For temporal discretisation (hybrid RANS/LES and LES), a second-order implicit scheme was applied. An implicit time stepping technique was chosen to guarantee stability for large CFL number. The time step was, however, chosen small enough so that the CFL-number in LES zones was at maximum 2, so that the dissipation due to the time stepping remained small. At each time step, inner iteration steps were applied to lower the residuals for the momentum and the transport equations below  $10^{-5}$ .

For the hybrid RANS/LES and LES model simulations the computational grids have been refined in the shear layer of the jet and in the near-wall regions as shown in Fig. 2. For the hybrid RANS/LES and RANS model computations the maximum value of  $y^+$  was less than 1 at the impingement plate, and less than 3 at the confinement plate. In LES,  $y^+ < 3$  at all walls. The numbers of grid points are summarized in Table 1. The LES model simulation has been

performed on the finest grid listed in Table 1, consisting of 15.1 million grid points. The RANS simulations have been performed on 2D grids which are cuts in the x-y plane of the 3D grids used for the hybrid RANS/LES model simulations. We refer to our previous work (Kubacki and Dick, 2009) for a discussion of the grid independence in the simulations with the RANS model.

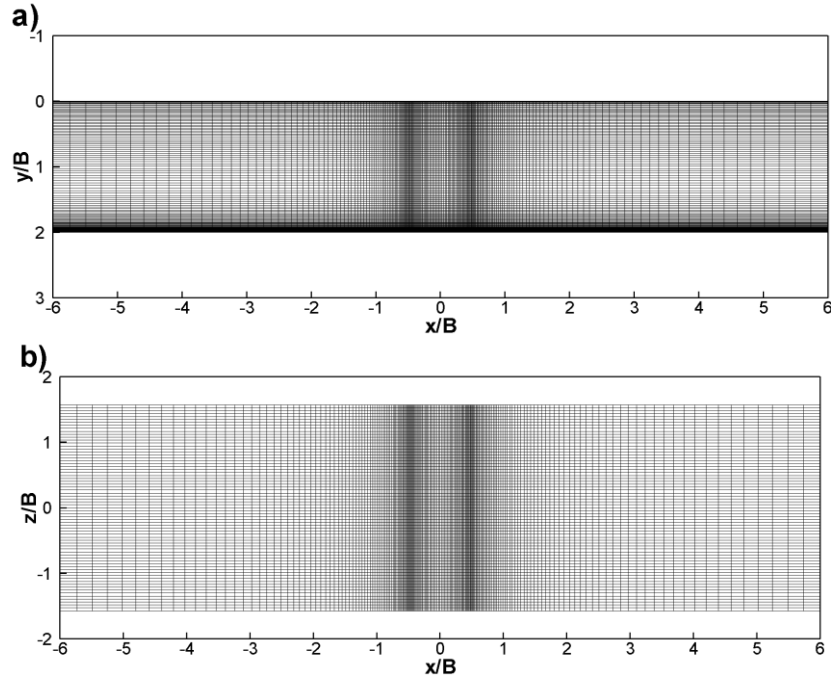


Figure 2. View of the computational mesh (a) in the x-y plane and (b) in the x-z plane (impingement plate) for simulation with the hybrid RANS/LES model ( $H/B=2$ ).

## RESULTS

### Inlet conditions

This section provides a verification of the two types of inlet conditions for simulation of the plane impinging jet with the hybrid RANS/LES model. The first way is using constant values of the turbulent kinetic energy,  $k$ , and the turbulent length scale,  $l_t$ , at the nozzle exit. The second way is using the exact shape of the inlet  $k$ -profile (as measured by Ashforth-Frost et al., 1997), together with a constant value of the turbulent (integral) length scale. The numerical results obtained with the hybrid RANS/LES model (impinging jet with the flat plate) are compared with the free jet flow measurements (Zhe and Modi, 2001), so in absence of the impingement plate. Note the similar turbulent intensity level at the jet exit in the measurements by (Zhe and Modi, 2001, and Ashforth-Frost et al., 1997).

Panels a and b of Fig. 3 show the mean axial and fluctuating axial velocity components at distance  $y/H=0.3$  from the nozzle exit for uniform profiles of the turbulent kinetic energy and the turbulent length scale over the inlet plane. The profiles have been averaged in time, in the spanwise  $z$  direction, and for positive and negative values of the  $x$ -coordinate with respect to the symmetry plane. It means that the numerical profiles have symmetry in Fig. 3 (also in Fig. 4, later). The computed mean velocity profile agrees well with the measured mean velocity (Fig. 3 a). This justifies the selection of the exponent in Eq. (6). The predicted fluctuating velocity profile (Fig. 3 b) is in good agreement with measured fluctuating velocity over 60% of the jet width, but some underprediction of the peak values is observed.

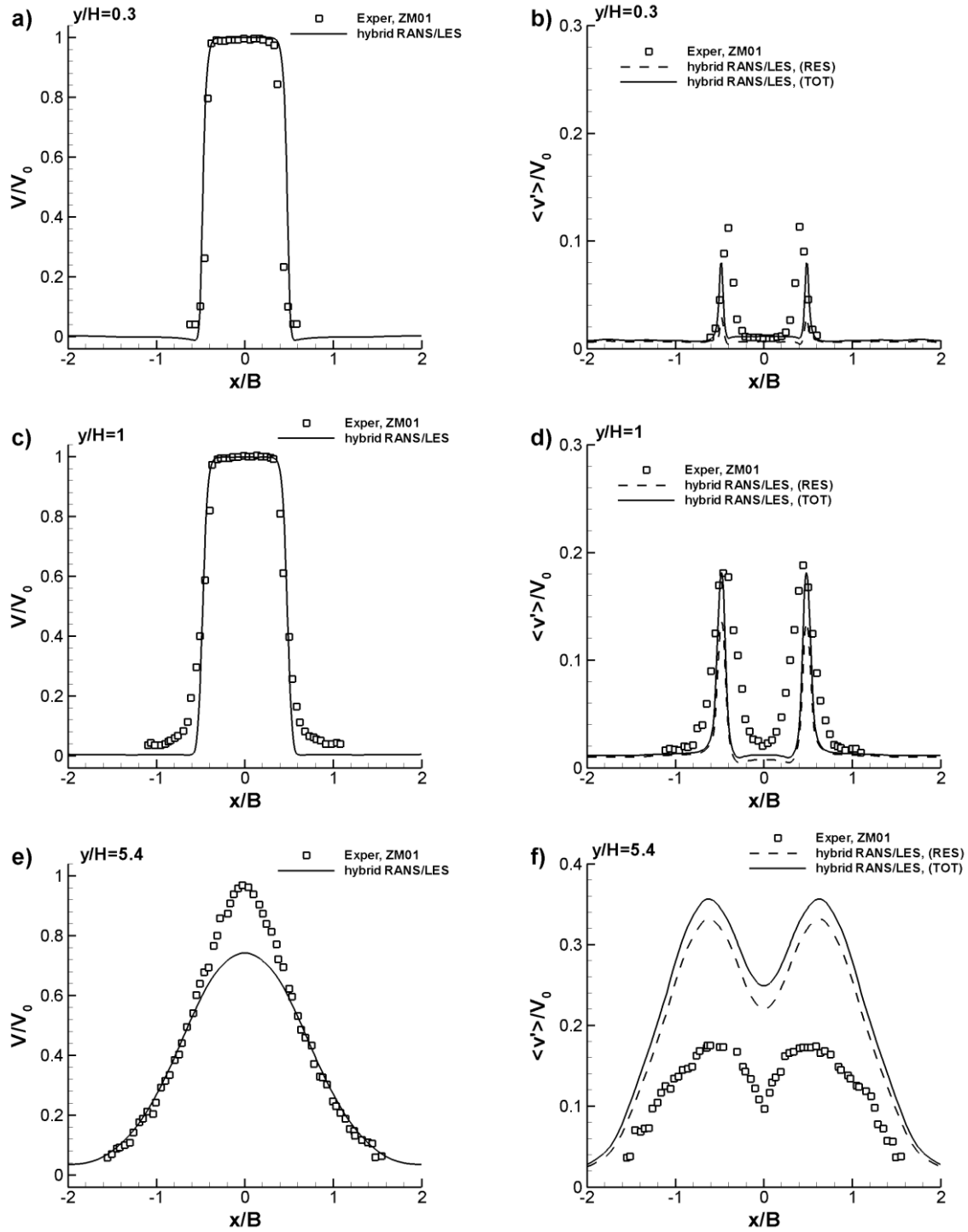


Figure 3. Profiles of mean axial velocity (a,c,e) and r.m.s. of axial fluctuating velocity component (b,d,f) for simulation of the plane impinging jet at  $H/B=9.2$ ,  $Re=20000$  at various distances from the jet exit: (a,b)  $y/H=0.3$ , (c,d)  $y/H=1$ , (e,f)  $y/H=5.4$  and comparison with experiment (free jet). The resolved and total (resolved+modelled) velocity fluctuations are denoted by RES and TOT, respectively.

The peak values of  $v'/V_0$  are better captured with the hybrid model further downstream at  $y/H=1$  as shown in Fig. 3 (d), but the width of the turbulent shear layer is underestimated. The

magnitude of the resolved fluctuating velocity at  $x/B=\pm 0.5$  is significantly higher at distance  $y/H=1$  (Fig. 3 d) than immediately following the jet exit,  $y/H=0.3$  (Fig. 3 b). This demonstrates that the hybrid model functions properly as the magnitude of the resolved scales gets higher with increasing distance from the jet exit, so when the width of the shear layer grows as a result of the Kelvin-Helmholtz instability. Further downstream ( $y/H=5.4$ ), the jet spreads strongly (Fig. 3 e and f). In the simulations, the decay of the mean velocity is much stronger than in experiment. This is accompanied by an abrupt increase of the fluctuating velocity level (Fig. 3 f). The predicted mean and fluctuating velocity characteristics at distance  $y/H=5.4$ , so in the middle between the nozzle exit and the impingement plate, cannot be directly compared with the experimental results by (Zhe and Modi, 2001) due to the effect of the impingement plate in the simulations. The impingement plate causes a strong flow recirculation inside the channel, leading to enhanced turbulent mixing in the jet flow region. Such flow recirculation is not present in the free jet flow. Overall, we observe good agreement between predicted and measured profiles of mean and fluctuating velocity at  $y/H=0.3$  and 1 (Fig. 3 a-d), especially in the jet core region at  $y/H=0.3$ , which means that the inlet conditions have been set correctly.

Next, the effect of the inlet profiles of the turbulent kinetic energy is demonstrated in Fig. 4. Two ways of specifying the inlet conditions for the turbulent quantities are studied here. The first way consist of using uniform profiles of turbulent kinetic energy and turbulent length scale over the inlet plane (as done above), while the second way consists of using the exact shape of the inlet profile of the turbulent kinetic energy (reproduced from Ashforth-Frost et al., 1997), together with a constant value of the integral length scale. Improved results are obtained in the simulation with the hybrid model immediately downstream of the slot ( $y/H=0.3$ ) using the exact shape of  $k$ -profile, but further downstream ( $y/H=1$ ) a slightly too small width of the shear layers of the jet is still apparent. Fig. 4 demonstrates that for the case studied here (almost flat inlet mean velocity profile) the form of the inlet profile of  $k$  has only a secondary effect on the width of the turbulent shear layers downstream of the slot, provided the bulk values of the turbulent quantities are set correctly. This justifies the selection of uniform profiles of the turbulent quantities for the hybrid RANS/LES and LES model simulations discussed below.

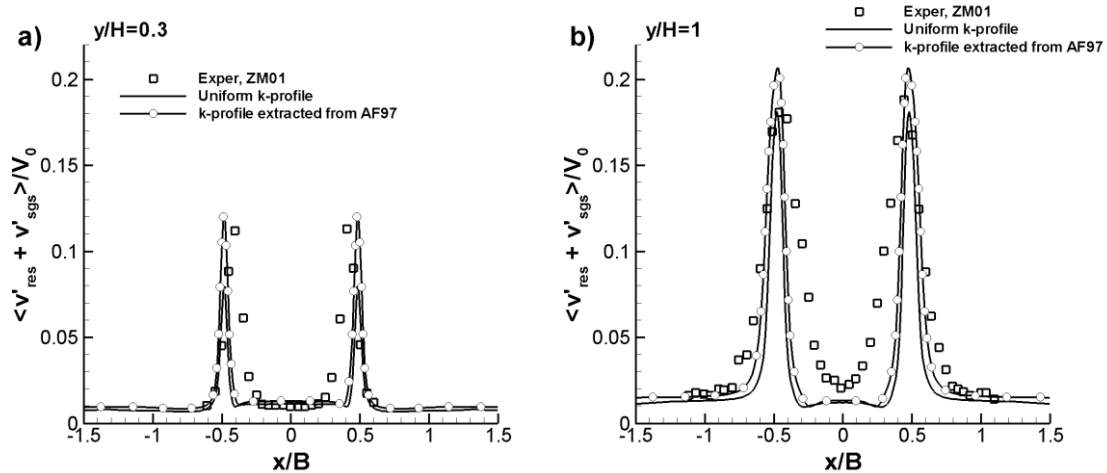


Figure 4. Profiles of axial fluctuating velocity component at distance  $y/H=0.3$  (a) and  $y/H=1$  (b) from the jet exit for simulation of the plane impinging jet at  $H/B=9.2$ ,  $Re=20000$  with uniform and variable inlet profile of turbulent kinetic energy.

### Low Reynolds number case

This section gives an analysis of the numerical results obtained with the RANS, hybrid RANS/LES and LES models for simulation of the plane impinging jet at  $H/B=2$  and  $Re=10000$ . The LES with the dynamic Smagorinsky model is performed on a very fine grid consisting of 15.1M grid points. The LES results are used as reference data for comparison with the results obtained using the RANS and hybrid RANS/LES models. The numerical results are also compared with experimental data by (Zhe and Modi, 2001).

Fig. 5 shows the mean streamwise velocity and fluctuating streamwise and wall-normal velocity components along the line perpendicular to the impingement plate at distance  $x/B=1$  from the symmetry plane. For the hybrid and LES methods, the mean and fluctuating velocity data have been averaged in time and in the spanwise  $z$  direction.

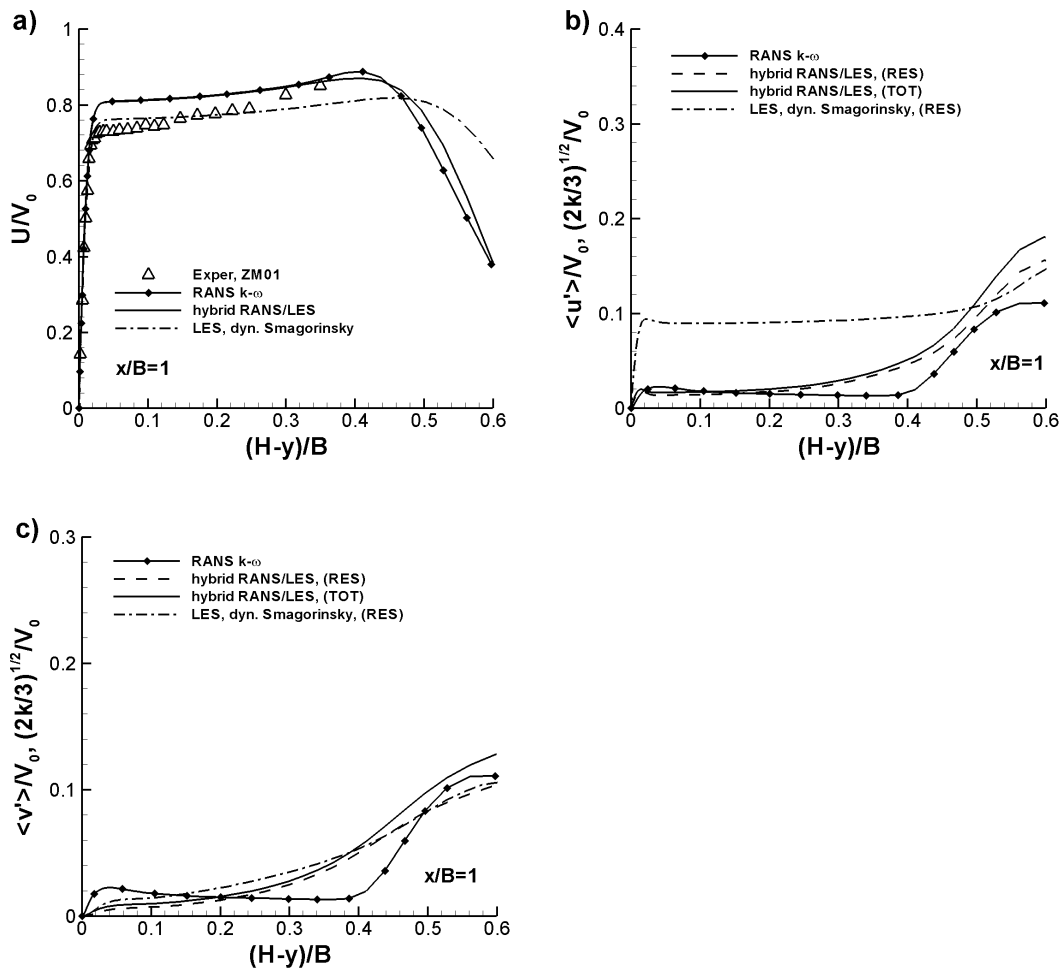


Figure 5. Profiles of mean streamwise velocity (a), streamwise fluctuating (b) and wall-normal (c) fluctuating velocity components for plane impinging jet simulation at  $H/D=2$ ,  $Re=10000$  at distance  $x/B=1$  from the symmetry plane.

With RANS, the fluctuating velocities are computed by  $u' = v' = (2k/3)^{1/2}$ . Fig. 5 (a) shows that the mean velocity profiles obtained with the RANS and hybrid RANS/LES models are quite similar to the results of the LES and that they are in good agreement with the experiment. The LES results are in better agreement with the experimental data close to the wall owing to the fine grid applied there. Some differences between the different modelling techniques can be observed in Fig. 5 (b) and (c), showing the fluctuating velocity components. Note that in case of the LES only the resolved fluctuations are shown. The hybrid RANS/LES model gives a

much smaller level of the streamwise fluctuating component than LES, but very much comparable to that obtained with RANS. The wall-normal fluctuating velocity obtained with the hybrid model is close to the wall-normal fluctuating velocity reproduced using LES. A similar level of the fluctuating velocities is reproduced with all modelling techniques in the outer part of the developing wall jet, which shows that the flow dynamics is well captured in the shear layers of the jet for the small nozzle-plate distance discussed here.

Further downstream (Fig 6 a), some differences are visible on the mean velocity profiles predicted with RANS and computed with the hybrid RANS/LES and LES models. The close-up view of the near-wall region shows that RANS gives a too steep velocity gradient close to the wall, while the results of the hybrid RANS/LES model are in good agreement with the experimental data. The near-wall velocity gradient obtained with LES is slightly too small. The near-wall peak of the streamwise fluctuating velocity is well reproduced with the hybrid RANS/LES model (Fig. 6 b). LES reproduces a too high level of streamwise fluctuating component which leads to a too strong momentum reduction in the near-wall region (Fig. 6 a).

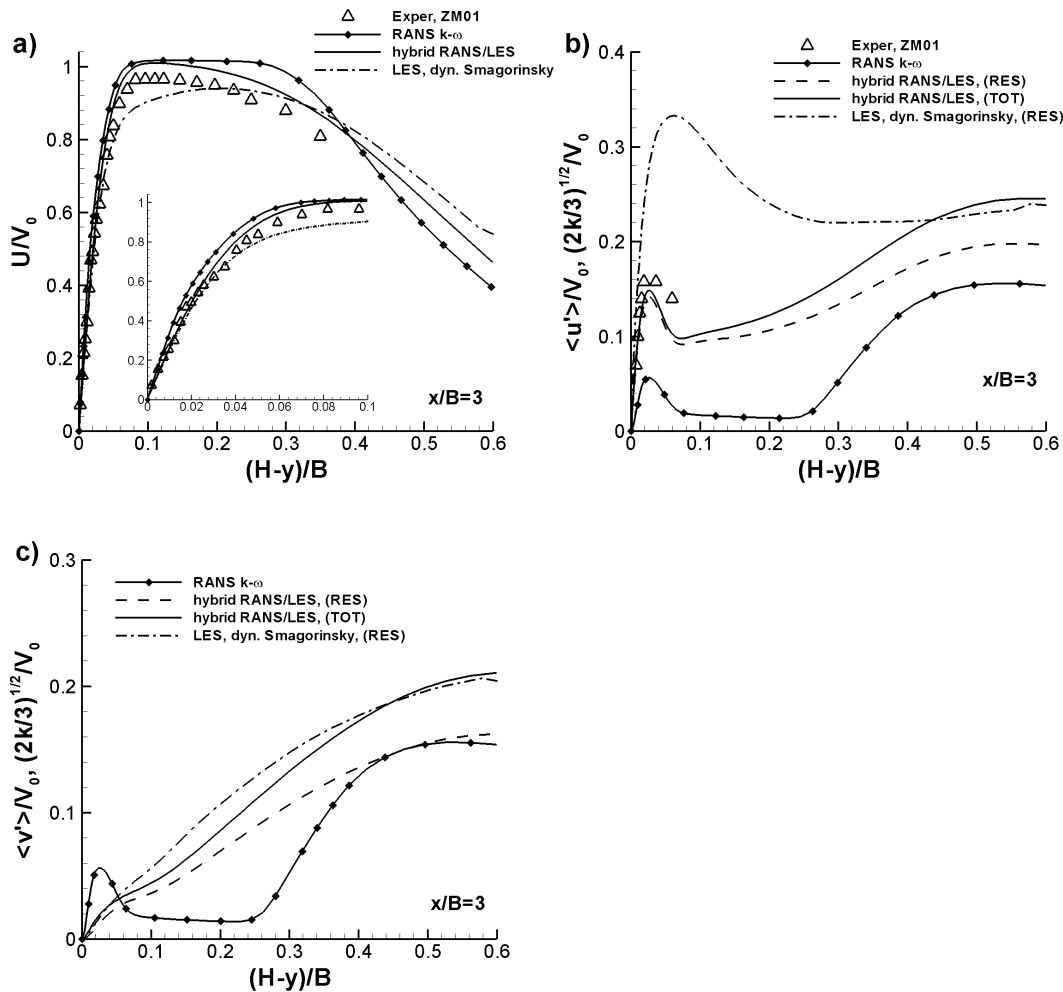


Figure 6. Profiles of mean streamwise velocity (a), streamwise fluctuating (b) and wall-normal (c) fluctuating velocity components for plane impinging jet simulation at  $H/B=2$ ,  $Re=10000$  at distance  $x/B=3$  from the symmetry plane.

Fig. 7 shows the mean and fluctuating velocity profiles at  $x/B=5$ . Significant differences are observed here, between results obtained using the different modelling techniques. First of all, the distance  $x/B=5$  seems to be already quite far from the symmetry plane for LES to be reliable. Note again that the grid cells become more and more anisotropic (Fig. 2) with



increasing distance from the symmetry plane. RANS overpredicts the peak value of the mean velocity, while the hybrid RANS/LES model seems to agree best with measurements by (Zhe and Modi, 2001). The overprediction of the fluctuating velocity components by LES can be explained by insufficient resolution to capture the final breakup phase of the vortex structures. It means that they are represented somewhat too large in the computation. This gives too large fluctuations. Similar conclusions were drawn by (Chaouat and Schiestel, 2005) for LES of fully-developed turbulent channel flow. The LES technique of Chaouat and Schiestel was based on transport equations for the subgrid-scale stresses. The coarse grid LES results by Chaouat and Schiestel showed overprediction of the total streamwise stresses. The results improved on a finer grid. The overprediction was explained by too large discretization errors (increased numerical diffusion) on a coarse grid which resulted in too large resolved structures. The results by (Chaouat and Schiestel, 2005), support our observation that the grid has to be fine enough to capture the velocity characteristics along the impingement plate with the dynamic Smagorinsky model. The current simulation results show, however, less sensitivity to the grid density with the hybrid RANS/LES models than with the LES model. So, we have to accept that LES is reliable only in a limited zone of the developing wall-jet region, so for  $x/B < 2$ .

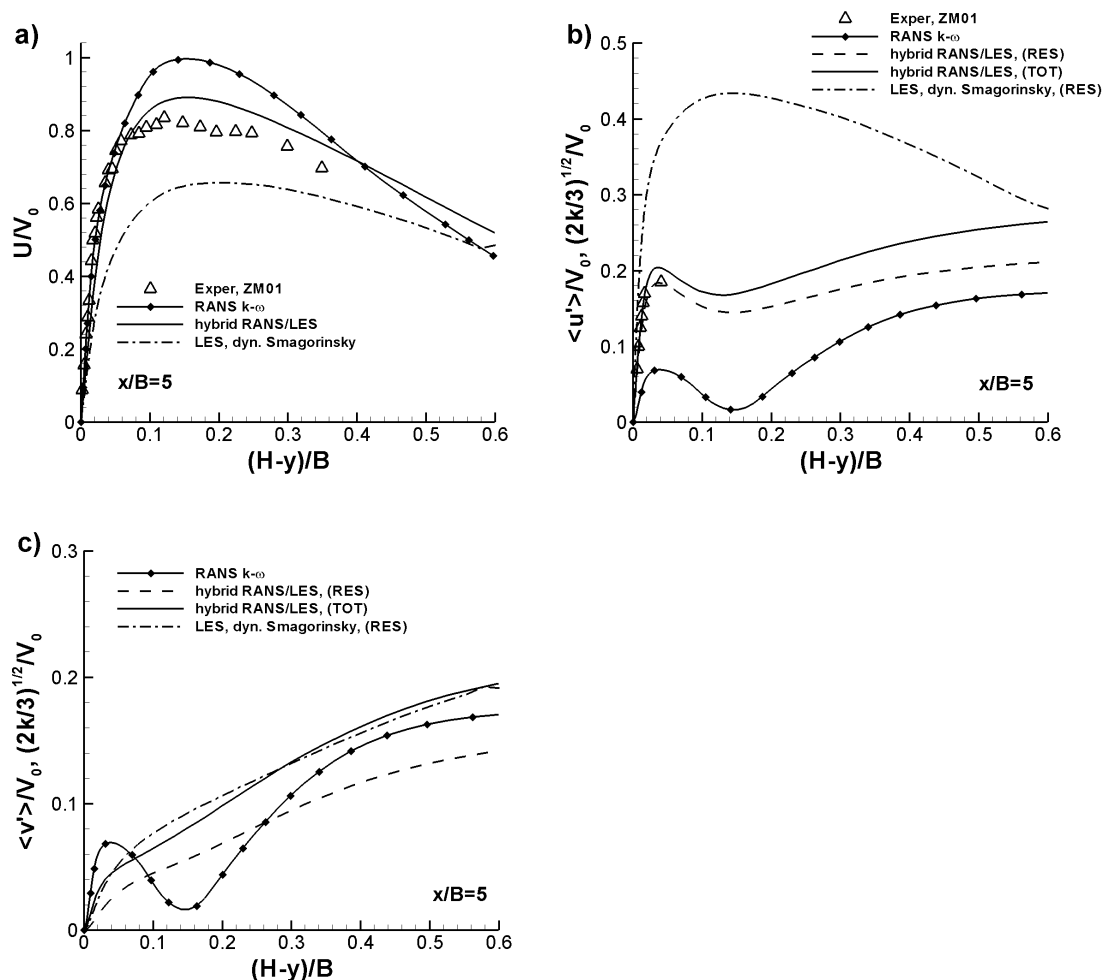


Figure 7. Profiles of mean streamwise velocity (a), streamwise fluctuating (b) and wall-normal (c) fluctuating velocity components for plane impinging jet simulation at  $H/B=2$ ,  $Re=10000$  at distance  $x/B=5$  from the symmetry plane.

The profile of the skin friction coefficient is displayed in Fig. 8. The peak values obtained using RANS and the hybrid model are very similar to the peak value obtained using LES. RANS overpredicts the skin friction coefficient in the developing wall jet region ( $x/B > 2$ ), owing to a too high momentum near the wall, as shown in Fig. 6 (a) and Fig. 7 (a). For  $x/B > 2$ , the skin friction profile reproduced with the hybrid RANS/LES model falls in between the skin friction profile obtained using RANS and LES. Again, we have to accept that the skin friction profile produced by LES is somewhat too low at distance  $x/B > 2$  due to lack of the grid resolution. Based on Fig. 6 (a) and Fig. 7 (a), which show that the velocity gradient near the wall obtained by the hybrid model compares very well with the experiments, we can conclude that the skin friction produced by the hybrid model is basically correct (we do not have explicitly the skin friction from the experiments).

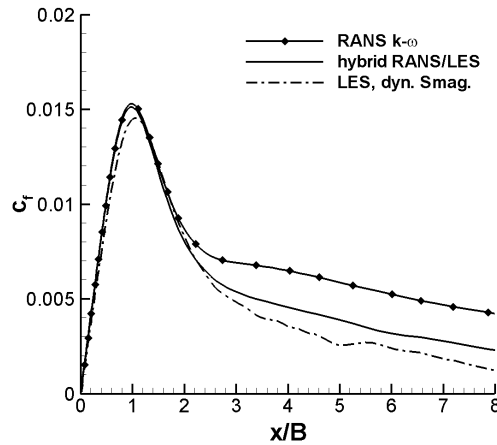


Fig. 8. Skin friction coefficient for  $H/B=2$ ,  $Re=10000$ .

The correspondence between the hybrid RANS/LES and LES model results is further analysed in Fig. 9 showing the contour plots of the Q-criterion ( $Q=1/2(\Omega_{ij}\Omega_{ij}-S_{ij}S_{ij})$ ) in the x-z plane (horizontal plane) at distance  $(H-y)/B=0.02$  from the impingement plate, obtained with the LES and the hybrid RANS/LES models. Both the LES and hybrid RANS/LES models reproduce the formation of spanwise-oriented vortex structures in the near-wall region of the developing wall jet at  $1 < |x/B| < 3$ . At first sight, the small-scale dynamics seems to be better captured with LES than with the hybrid model at  $|x/B| > 3$ . This is due to higher grid resolution in the spanwise z direction which allows formation of smaller structures in case of the LES model (Table 1). The distance  $(H-y)/B=0.02$  is very close to the wall, so most of the near-wall turbulence resides in RANS mode there in the hybrid model. More specifically, it means that the ratios of the modelled to the RANS eddy viscosity,  $\nu_t/\nu_{RANS}$  (where  $\nu_{RANS}=k/\omega$ ) and the LES length scale to the turbulent length scale,  $\min(C_{DES}\Delta/L_t, 1)$ , are equal to unity (results not shown here) over the complete x-z plane (Fig. 9). As a result, the modelled turbulence is somewhat larger with the hybrid model than with LES in the near-wall region of the developing wall-jet (Fig. 10), which compensates for the reduced activity of the small, resolved LES-like structures using the hybrid model. A verification of the fluctuating velocity components in Fig 6 (b) and Fig. 7 (b) allows to conclude that LES gives a wealth of the streamwise-oriented structures in Fig. 9 (a) at distance  $|x/B| > 3$  which are reproduced somewhat a too big. As mentioned, this is due to a grid coarsening with increasing distance from the symmetry plane.

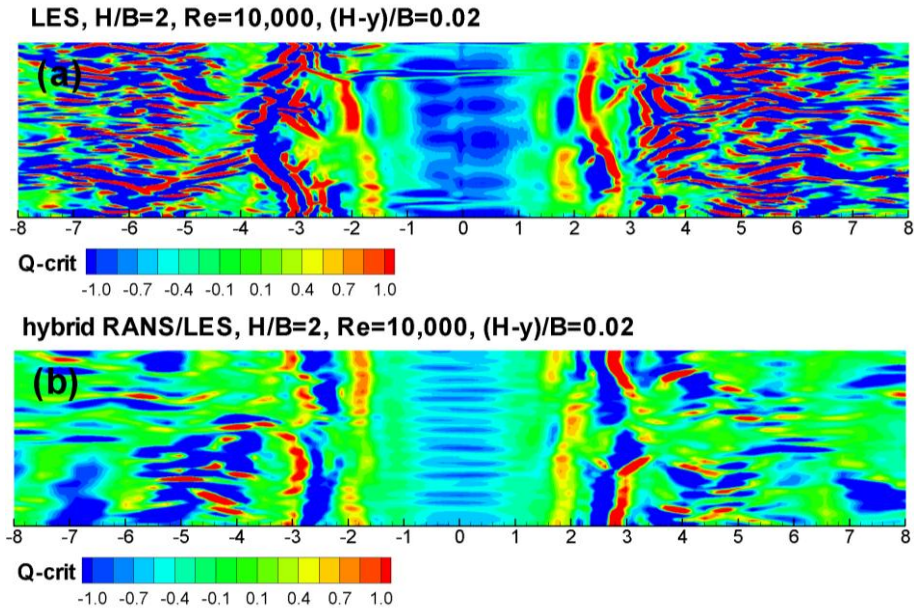


Figure 9. Contour plots of Q-criterion in the x-z plane at distance  $(H-y)/B=0.02$  from the impingement plate obtained with (a) LES (15.1M cells) and (b) hybrid RANS/LES model (2.5M cells).

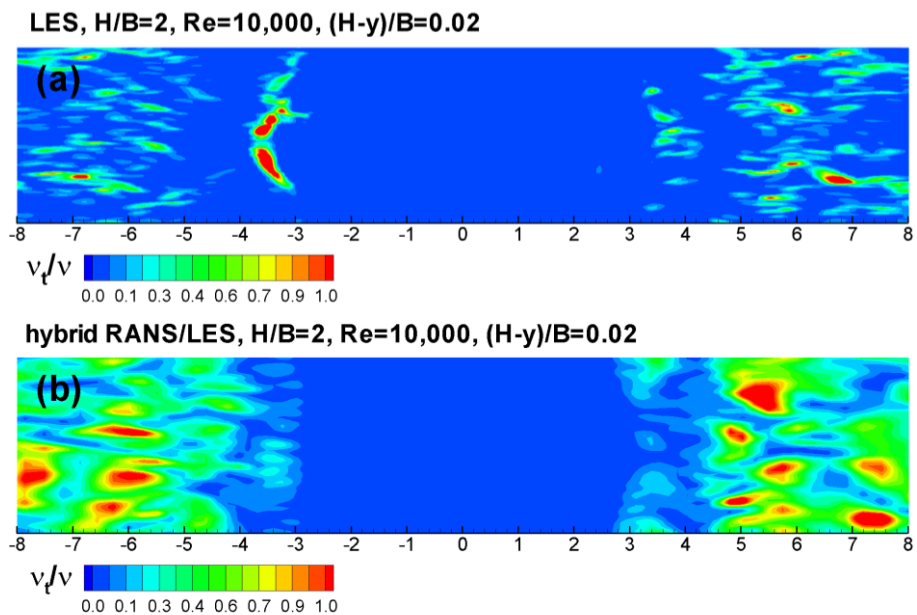


Figure 10. Contour plots of ratio of modelled to molecular viscosity in the x-z plane at distance  $(H-y)/B=0.02$  from the impingement plate obtained with (a) LES (15.1M cells) and (b) hybrid RANS/LES model (2.5M cells).

### High Reynolds number case

The present section discusses the mean and fluctuating velocity characteristics in the near-wall region of the developing wall jet for simulation of the plane impinging jet at  $H/B=4$ ,  $Re=18000$  with the  $k-\omega$  RANS and the hybrid RANS/LES models. The numerical results are compared with experimental data by (Zhe and Modi, 2001, Ashforth-Frost et al., 1997 and Dogruoz, 2005). As shown in Fig. 11 (a, c) and (e) the streamwise velocity profiles

reproduced with the  $k-\omega$  RANS model are in good agreement with measured velocity profiles except very near to the wall where RANS gives a too steep velocity gradient.

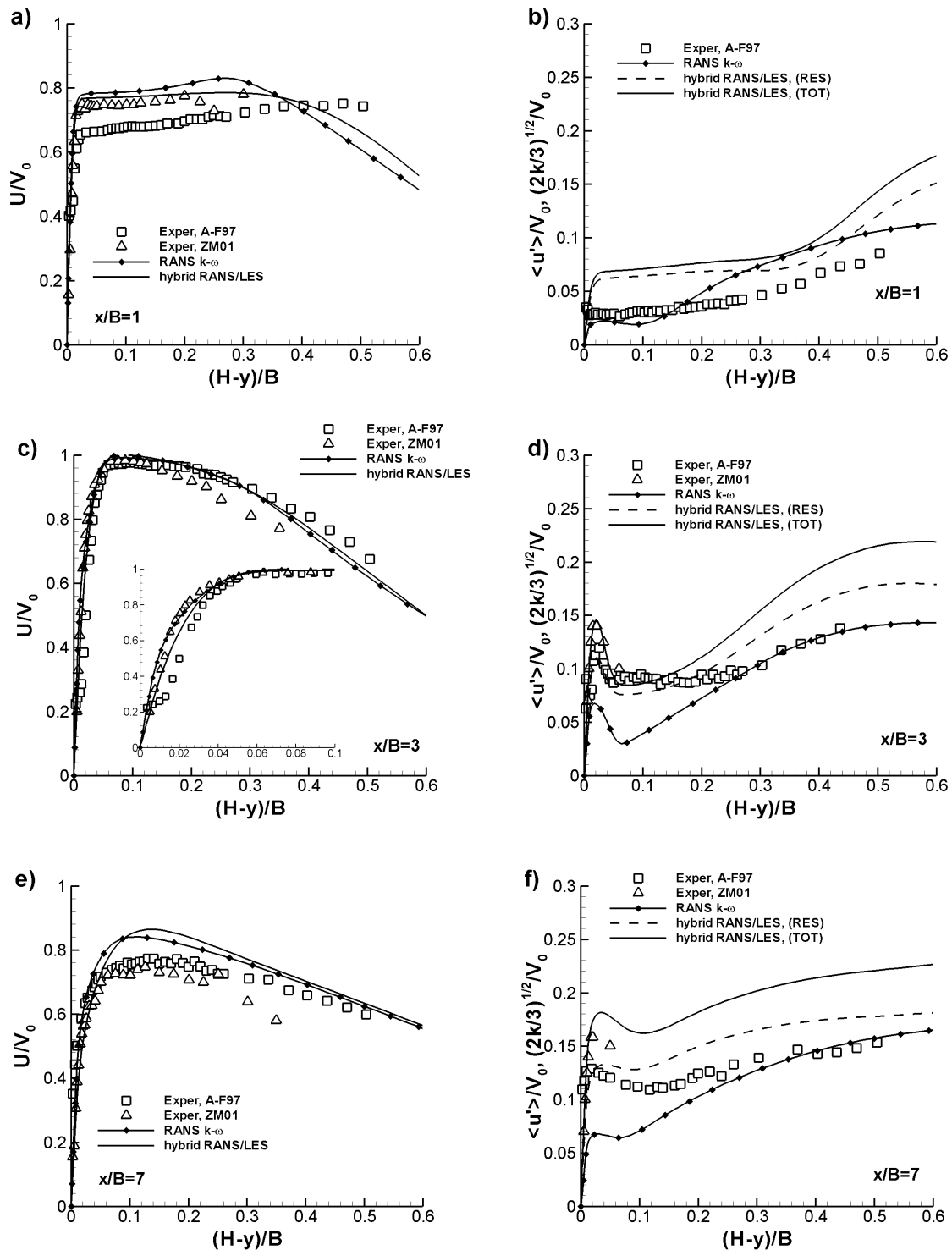


Figure 11. Profiles of mean streamwise velocity (a,c,e) and r.m.s. of streamwise fluctuating velocity component (b,d,f) for simulation of the plane impinging jet at  $H/D=4$ ,  $Re=18000$  at various distances from the symmetry plane: (a,b)  $x/B=1$ , (c,d)  $y/B=3$  and (e,f)  $y/B=7$ . In case of the hybrid model the resolved and total (resolved+modelled) fluctuations are denoted by RES and TOT, respectively.

The near-wall behaviour is better captured with the hybrid RANS/LES model. This is demonstrated in the close-up view of the near-wall region shown in Fig. 11 (c). Panels b, d and f of Fig. 11 show the comparison between numerical and measured fluctuating streamwise velocity components. The measured wall-normal fluctuating components are not available for this test case, but from Fig 11 (b) we can speculate that RANS slightly overpredicts the turbulent kinetic energy in the impact zone. The hybrid RANS/LES model gives a too high streamwise fluctuating velocity at  $y/B=1$  (Fig. 11 b), but the near-wall fluctuating velocity is much better captured with the hybrid model further away from the symmetry plane (Fig. 11 d and f). The hybrid model has a tendency to reproduce a too high level of fluctuating velocity away from the wall ( $(H-y)/B > 0.2$ ). This might be an indication that the vortex structures produced by the hybrid model are too large there.

Fig. 12 shows the skin friction coefficient along the impingement plate for  $H/B=4$ ,  $Re=18000$ . The numerical results are compared with experimental data by (Dogruoz, 2005). RANS is in error in the transition zone ( $2 < x/B < 7$ ), both 2D RANS and 3D RANS. With the hybrid model, the deficiency is cured.

Summing up, the hybrid RANS/LES model gives realistic mean and fluctuating velocity profiles along the impingement plate at  $H/B=4$ ,  $Re=18000$ . The RANS model has the tendency to overpredict the mean velocity gradient in the near-wall region of the developing wall jet. The dip in the skin friction profile is not captured using RANS despite the stress-limiter (Eq. 5). It means that the stress-limiter is not sufficiently strong in the developing wall jet region. The flow details in the transition from the stagnation flow to the developed wall jet region are much better reproduced with the hybrid RANS/LES model than using RANS.

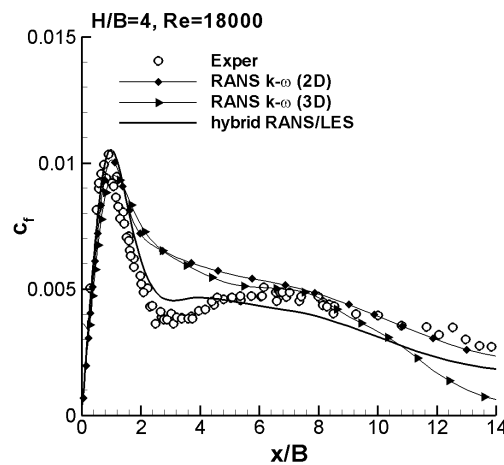


Fig. 12. Skin friction coefficient for  $H/B=4$ ,  $Re=18000$

## SUMMARY

The results of simulations of plane impinging jets at different nozzle-plate distances ( $H/B=2, 4$  and  $9.2$ ) and three Reynolds numbers ( $Re=10000, 18000, 20000$ ) using a  $k-\omega$  based hybrid RANS/LES model were presented. The  $k-\omega$  RANS model has been employed for the low nozzle-plate distance cases ( $H/B=2$  and  $4$ ). Reference results using LES with the dynamic Smagorinsky model were generated for  $H/B=2$ ,  $Re=10000$ .

Overall, good agreement with the experimental data of (Zhe and Modi, 2001) has been obtained with the hybrid RANS/LES model for jet impingement at  $H/B=4$  and  $Re=18000$  in terms of the mean and fluctuating velocity profiles along the plate. Very good agreement between computed and measured skin friction coefficient along the impingement plate has been obtained with the hybrid RANS/LES model for  $H/B=4$ ,  $Re=18000$ . The hybrid model

results agree also well with the reference LES results in the stagnation flow region ( $x/B < 2$ ) for  $H/B=2$ ,  $Re=10000$ . With the RANS model, the stress-limiter is not strong enough, leading to a too large wall shear stress reproduced with RANS along the impingement plate.

## ACKNOWLEDGEMENTS

The first author acknowledges an international cooperation grant of Ghent University and the support from a research project funded by the Polish National Science Centre (decision number DEC-2011/01/B/ST8/07267).

## REFERENCES

- Ashforth-Frost S., Jambunathan K., Whitney C.F. (1997): *Velocity and turbulence characteristics of a semiconfined orthogonally impinging slot jet*, Experimental Thermal and Fluid Science, Vol. 14, pp. 60-67.
- Beaubert F., Viazzo S., (2003): *Large eddy simulations of plane turbulent impinging jets at moderate Reynolds numbers*, Int. J. Heat Fluid Flow, Vol. 24, pp. 512-519.
- Chaouat B., Schiestel R. (2005): *A new partially integrated transport model for subgrid-scale stresses and dissipation rate for turbulent developing flows*, Phys. Fluids, Vol. 17, 065106.
- Cziesla T., Biswas G., Chattopadhyay H., Mitra N.K. (2001): *Large-eddy simulation of flow and heat transfer in an impinging slot jet*, Int. J. Heat Mass Transfer, Vol. 22, pp. 500-508.
- Davidson L., Peng S.H. (2003): *Hybrid LES-RANS modelling: a one-equation SGS model combined with a  $k-\omega$  model for predicting recirculating flows*, Int. J. Numer. Meth. Fluids, Vol. 43, pp. 1003-1018.
- Dogruoz M.B. (2005): *Experimental and Numerical Investigation of Turbulent Heat Transfer due to Rectangular Impinging Jets*, Ph.D. Thesis, The University of Arizona, Tucson, Arizona.
- Fernandez J.A., Elicer-Cortes J.C., Valencia A., Pavageau M., Gupta S. (2007): *Comparison of low-cost two-equation turbulence models for prediction flow dynamics in twin-jets devices*, Int. Commun. Heat Mass Transfer, Vol. 34, pp. 570-578.
- Fröhlich J. von Terzi D. (2008): *Hybrid LES/RANS methods for the simulation of turbulent flows*, Progress in Aerospace Sciences, Vol. 44, pp. 349–77.
- Guo Y., Wood D.H. (2002): *Measurements in the vicinity of a stagnation point*, Experimental Thermal and Fluid Science, Vol. 25, pp. 605–614.
- Hattori H., Nagano Y. (2004): *Direct numerical simulation of turbulent heat transfer in plane impinging jet*, Int. J. Heat Fluid Flow, Vol. 25, pp. 749-758.
- Jaramillo J.E., Perez-Segarra C.D., Rodriguez I., Oliva A. (2008): *Numerical study of plane and round impinging jets using RANS models*, Numer. Heat Transfer Part B, Vol. 54, pp.213-237.
- Kok J.C., Dol H., Oskam H., van der Ven H. (2004): *Extra-large eddy simulation of massively separated flows*, AIAA Paper 2004-0264.
- Kubacki S., Dick E. (2009): *Convective heat transfer prediction for an axisymmetric jet impinging onto a flat plate with an improved  $k-\omega$  model*, Int. J. Numer. Methods in Heat and Fluid Flow, Vol. 19, pp. 960-981.
- Kubacki S., Dick E. (2010): *Simulation of plane impinging jets with  $k-\omega$  based hybrid RANS/LES models*, Int. J. Heat Fluid Flow, Vol. 31, pp. 862-878.

- Kubacki S., Dick E. (2011): *Hybrid RANS/LES of flow and heat transfer in round impinging jets*, Int. J. Heat Fluid Flow, Vol. 32, pp. 631-651.
- Mathey F., Cokljat D., Bertoglio J.P., Sergeant E. (2006): *Assessment of the vortex method for Large Eddy Simulation inlet conditions*, Progress Comput. Fluid Dynamics, Vol. 6, pp. 58-67.
- Narayanan V., Seyed-Yagoobi J., Page R.H. (2004): *An experimental study of fluid mechanics and heat transfer in an impinging slot jet flow*, Int. J. Heat and Mass Transfer, Vol. 47, pp. 1827–1845.
- Sakakibara J., Hishida K., Maeda M. (1997): *Vortex structure and heat transfer in the stagnation region of an impinging plane jet (simultaneous measurements of velocity and temperature fields by digital particle image velocimetry and laser-induced fluorescence)*, Int. J. Heat Mass Transfer, Vol. 40, pp. 3163-3176.
- Scotti A., Meneveau C., Lilly D.K. (1993): *Generalized Smagorinsky model for anisotropic grids*, Phys. Fluids A, Vol. 5, pp. 2306–2308.
- Senter J., Sollic C. (2007): *Flow field analysis of a turbulent slot air jet impinging on a moving flat surface*, Int. J. Heat Fluid Flow, Vol. 28, pp. 708-719.
- Spalart P.R., Deck S., Shur M.L. Squires K.D., Strelets M, Travin A. (2006): *A new version of detached-eddy simulation, resistant to ambiguous grid densities*, Theor. Comput. Fluid Dyn., Vol. 20, pp. 181-195.
- Strelets M. (2001): *Detached eddy simulation of massively separated flows*, AIAA Paper 2001-0879, 2001.
- Tu C.V., Wood D.H., (1996): *Wall pressure and shear stress measurements beneath an impinging jet*, Experimental Thermal and Fluid Sci., Vol. 13, pp. 364-373.
- Tsubokura M., Kobayashi T., Taniguchi N., Jones W.P. (2003): *A numerical study on the eddy structures of impinging jets exited at the inlet*, Int. J. Heat Fluid Flow, Vol. 24, pp. 500-511.
- Wilcox D.C. (2008): *Formulation of the  $k-\omega$  turbulence model revisited*, AIAA Journal Vol. 46, pp. 2823-2837.
- Yan J., Mocket C., Thiele F. (2005): *Investigation of alternative length scale substitutions in detached-eddy simulation*, Flow Turbulence and Combustion, Vol. 74, pp. 85-102.
- Zhe J., Modi V. (2001): *Near wall measurements for a turbulent impinging slot jet*, Trans. of the ASME, J. Fluid Eng. Vol. 123, pp. 112-120.